Electrical Cross-Correlation Spectroscopy: Measuring Picoliter-per-Minute Flows in Nanochannels

Klaus Mathwig, Dileep Mampallil, Shuo Kang, and Serge G. Lemay*

MESA+ Institute for Nanotechnology, University of Twente, PO Box 217, 7500 AE Enschede, The Netherlands
(Received 2 March 2012; revised manuscript received 27 June 2012; published 10 September 2012)

We introduce all-electrical cross-correlation spectroscopy of molecular number fluctuations in nanofluidic channels. Our approach is based on a pair of nanogap electrochemical transducers located downstream from each other in the channel. When liquid is driven through this device, mesoscopic fluctuations in the local density of molecules are transported along the channel. We perform a time-of-flight measurement of these fluctuations by cross-correlating current-time traces obtained at the two detectors. Thereby we are able to detect ultralow liquid flow rates below 10 pL/min. This method constitutes the electrical equivalent of fluorescence cross-correlation spectroscopy.

Systems in diffusive equilibrium undergo number fluctuations that encode a wealth of information on the underlying microscopic dynamics. This is explicitly exploited by methods such as fluorescence correlation spectroscopy [1,2] to extract molecular properties in a wide range of biophysics experiments [3]. Here we establish a new technique to electrically probe these number fluctuations using electrodes embedded in nanochannels. We demonstrate the utility of the method by measuring ultralow liquid flow rates.

The number N of solute molecules in a nanochannel volume fluctuates in time due to Brownian motion, thereby providing the basis for our measurement method. For a Poisson-distributed dilute solute, the ratio of noise to average number is $\sqrt{\langle (\Delta N)^2 \rangle}/\langle N \rangle = 1/\sqrt{\langle N \rangle}$. Therefore, the relative size of the fluctuations is usually too small to detect in macro- or even microscale volumes; this mesoscopic effect is in this sense a hallmark of nanofluidic systems.

To probe the fluctuations, we employ electrochemical nanofluidics devices, or nanogap transducers [4], as sketched in Fig. 1(a). Electrochemically active molecules transport electrons by shuttling between closely spaced (130 nm), facing electrodes embedded in the walls of a nanochannel. This repeated, alternating oxidation and reduction, known as redox cycling, allows each molecule to transport several thousand electrons per second, leading to a large enhancement of the detected electrochemical current (typically several femtoamperes per molecule). For the purpose of flow detection, this device fulfills a simple function: it yields an electrical current that is directly proportional to the number of electrochemically active molecules in the volume between the electrodes as a function of time. In the 10 fL detection volume of a device, there are about 9 000 000 molecules present at a 1 mM analyte concentration (mean electrical current of 45 nA). Their fluctuation of 3000 molecules leads to a current noise of 15 pA, which is easily detected.

Our experimental arrangement is shown in Fig. 1. Two electrodes at the top wall of a nanofluidic channel define two distinct detection volumes. A third electrode at the bottom wall of the channel allows redox cycling to take place in both volumes. Current-time traces are recorded simultaneously at both top electrodes. When liquid is driven through the channel, the analyte molecules' average velocity is equal to the average liquid flow velocity. If the flow is fast enough to outrun the molecules' longitudinal diffusion, the number fluctuations are preserved while they travel along the channel [5]. Therefore, the same noise that is measured at the first electrode is measured again a fraction of a second later at the second electrode
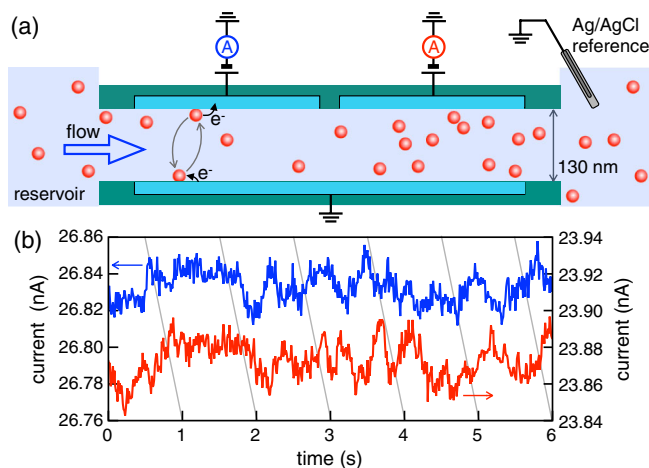

FIG. 1 (color online). (a) Schematic of the measurement concept. Fluctuations of the number of electrochemically active molecules are electrically measured at two electrodes in a nanochannel. Liquid flow velocity is determined by time-of-flight detection of these fluctuations as the molecules are transported along the channel from the upstream to the downstream transducer. (b) Raw current-time traces recorded at both electrodes at a flow rate corresponding to a time shift of approximately 0.2 s. Gray lines are guides to the eye.

downstream, as illustrated in Fig. 1(b). The time of flight from the center of the first electrode to the center of the second one is determined by evaluating the cross-correlation function $G_C(\tau)$ of the fluctuation $\delta I(t) = I(t) - \langle I \rangle$ for both current-time traces $I_{1,2}(t)$ (normalized to $G_C = 1$ for complete correlation),

$$G_C(\tau) = \langle \delta I_1(t) \delta I_2(t + \tau) \rangle / \langle \delta I_{1,2}^2 \rangle. \qquad (1)$$

$G_C(\tau)$ peaks at the time of flight, which is in a first approximation inversely proportional to the average liquid velocity.

Nanogap sensors were fabricated as described previously [4,6]. In short, the devices consist of a photolithographically defined 50 μm to 100 μm long, 5 μm wide and 130 nm high channel in silicon nitride fabricated on an oxidized silicon wafer. The channel volume was defined by a sacrificial Cr layer deposited by electron-beam evaporation that was wet etched directly before the experiment. A 3 μm wide Pt electrode was positioned on the channel floor, and two 5 μm wide and 24 μm to 49 μm long Pt electrodes separated by a 2 μm wide gap formed the channel ceiling. At both ends, access holes were dry etched through the silicon nitride passivation layer to open up the channel.

We chose a syringe pump (Pump 11 Pico Plus Elite, Harvard Apparatus) to drive liquid flow, because it is the most simple and direct way for the generation of very stable flows. It further requires only a minimum of fluid handling of small sample volumes, which can thus be well protected from the environment. However, low rates of picoliters per minute are too small to be delivered—it would take several years for a drop of water (30 μL) to pass through the nanochannel. Therefore we used the pump in a parallel flow control configuration [7,8]. Here an additional fluidic layer of microchannels in polydimethylsiloxane (PDMS) was bonded to the nanofluidic chip, so that a 100 μm long microchannel with a 3 μm $\times$ 5 μm cross section ran in parallel to the nanochannel, as shown in Fig. 2.
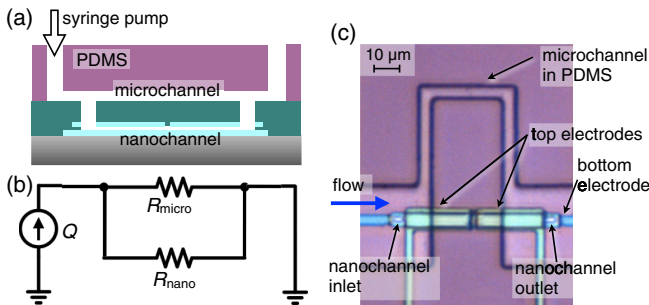

FIG. 2 (color online). (a) Schematic cross section of a nanofluidic device connected to a microchannel in a parallel flow control setup. (b) Equivalent fluidic circuit of the configuration. (c) Top view micrograph of a 50 μm long device bonded to a 100 μm long microchannel in PDMS.

For a Poiseuille flow in this parallel configuration, the ratio of both channels' flow rates Q scales as their hydraulic resistances R [9,10],

$$\frac{Q_{\text{micro}}}{Q_{\text{nano}}} = \frac{R_{\text{nano}}}{R_{\text{micro}}} \approx \frac{(1 - 0.630 h_m/w_m)}{(1 - 0.630 h_n/w_n)} \frac{h_m^3 w_m}{h_n^3 w_n} \frac{L_n}{L_m}, \quad (2)$$

with $L_{n,m}$, $w_{n,m}$ and $h_{n,m}$ being the nano- and microchannel's length, width and height, respectively. Due to the cubic dependence of flow on the channel height, a high ratio of approximately 8000:1 is achieved for a 100 μm long device. In practice, two devices, each with a microchannel, are connected in parallel; therefore, the nanochannel flow rate is reduced by a factor of 16 000 compared to the syringe flow [11].

Ferrocenedimethanol [Fc(MeOH)$_2$], purchased from Acros, with diffusion coefficient $D = 6.7 \times 10^{-10}$ m^2/s, was chosen as a redox-active species. A 1 mM solution was prepared in milli-Q water with 1 M KCl (Sigma-Aldrich) added as background electrolyte together with 5 mM H$_2$SO$_4$ (Sigma-Aldrich) to prevent electrode degradation. Prior to measurements, the microchannels were filled with chromium etchant (Selectipur from BASF) to remove the Cr sacrificial layer and release the nanogap devices. The etchant was then replaced with 5 mM H$_2$SO$_4$ and subsequently with the Fc(MeOH)$_2$-containing solution, which was then driven with varying pump flow rates of up to 50 μL/h.

Both top electrodes of the devices were connected to Keithley 6430 sub-femtoamp remote source meters. The two top electrodes were biased at an oxidizing potential of 0.4 V while the bottom electrode was short-circuited to a Ag/AgCl reference electrode connected by tubing downstream of the device. The whole setup was shielded in a Faraday cage. Current-time traces of 25 s with 10 ms sampling intervals were simultaneously recorded at the top electrodes, as illustrated in Fig. 1(b). High-pass filtering was applied to remove low-frequency (< 50 mHz) drift.

Cross-correlation functions of the traces were then determined for different pump flow rates, as shown in Fig. 3(a). These curves exhibit clear peaks at τ_{peak}, which shift to shorter times with faster flow such that $\tau_{\text{peak}} \propto$ (pump flow rate)$^{-1}$. This is expected since the molecules sample the cross section homogenously and Taylor dispersion is negligible at low Péclet numbers (Pé < 0.1); flow is laminar at Reynolds numbers Re $< 10^{-4}$ and electrokinetic effects are insignificant [11]. The decreased peak height and broadening of the peaks at low flow rates corresponds to a loss of correlation due to a more dominant influence of diffusion on the molecules' movement. This is straightforward to understand: for a pronounced peak to appear, the longitudinal rms fluctuation Δx of the molecules during the time of flight should be smaller than the center-to-center distance $L + g$ of the electrodes,
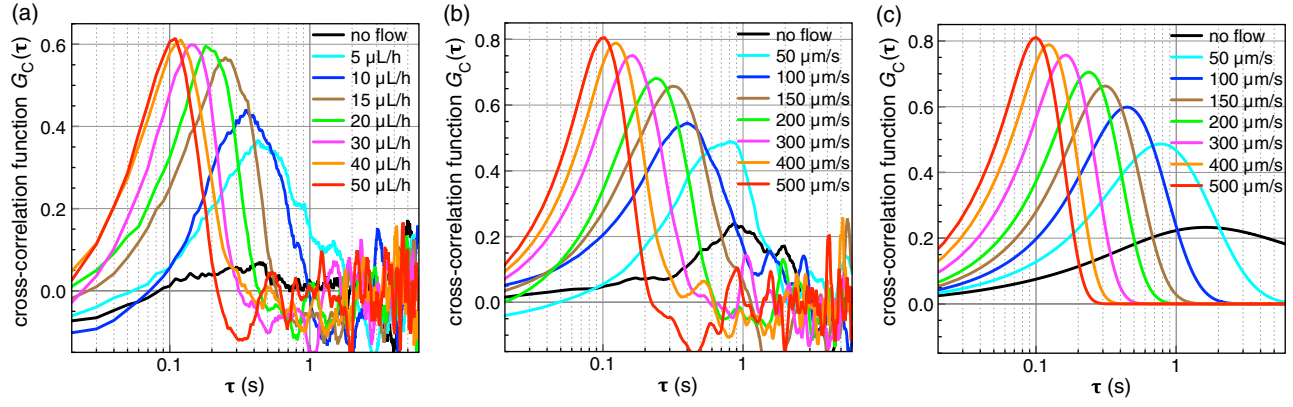
FIG. 3 (color online). (a) Cross-correlation functions of current-time traces recorded at the two 49 μm long top electrodes of a 100 μm long device for different pump flow rates. (b) Cross correlation of current-time traces generated by a one-dimensional random walk superimposed with flow for the same device geometry and diffusion coefficient. (c) Analytically derived cross-correlation functions for the same one-dimensional geometry and diffusion coefficient.

$\Delta x = \sqrt{2D\tau_{peak}} \ll L + g$. This leads to the condition $v \gg 2D/(L + g)$ for well-defined correlation peaks.

To test our hypothesis that the measured cross correlations can be understood simply as the superposition of longitudinal drift and diffusion, we performed a one-dimensional random walk simulation [12]. In short, 10 000 molecules were randomly distributed and underwent random steps at 1 μs intervals. An additional drift term was superimposed to represent the flow velocity v. At each time step, the number of molecules, or occupancy, in two regions of length $L = 49$ μm separated by a gap of $g = 2$ μm was evaluated in a 2 mm long geometry with closed-loop boundary conditions. Thirty seconds long occupancy traces were generated and then cross correlated in the same way as the experimentally obtained currents. The resulting cross-correlation functions for different flow velocities are shown in Fig. 3(b). They show good agreement with the experimental data, for example exhibiting similar noise at long times τ caused by the finite duration of the

traces. We attribute the slightly smaller peak height of the experimental data (~ 0.6 instead of 0.8) to asymmetrically fabricated top electrode areas.

To facilitate further analysis, we derived an analytical form of the cross-correlation function $G_C(L, g, D, v, \tau)$. In close analogy to two-beam cross-correlation spectroscopy [13], G_C was evaluated from the expression

$$G_C(\tau) = \frac{\int W_1(x)W_2(x')f(x, x', \tau)dxdx'}{\langle N \rangle^2 \int W_1(x)dx \int W_2(x')dx'}, \quad (3)$$

where $W_{1,2}(x)$ correspond to the detection regions defined by top electrodes and f is a number concentration correlation function, i.e., in essence the probability to find a molecule originally at the longitudinal position x a time τ later at x'. The details of the calculation are given in the Supplemental Material [11]. The resulting cross-correlation function is explicitly given by

$$G_C(\tau) = \sqrt{\frac{D\tau}{\pi L^2}}\left\{\exp\left[-\frac{(2L + g - v\tau)^2}{4D\tau}\right] + \exp\left[-\frac{(g - v\tau)^2}{4D\tau}\right] - 2\exp\left[-\frac{(L + g - v\tau)^2}{4D\tau}\right]\right\}$$
$$+ \frac{2L + g - v\tau}{2L}\,\mathrm{erf}\left(\frac{2L + g - v\tau}{\sqrt{4D\tau}}\right) + \frac{g - v\tau}{2L}\,\mathrm{erf}\left(\frac{g - v\tau}{\sqrt{4D\tau}}\right) - \frac{L + g - v\tau}{L}\,\mathrm{erf}\left(\frac{L + g - v\tau}{\sqrt{4D\tau}}\right). \quad (4)$$

$G_C(\tau)$ is shown in Fig. 3(c): it resembles a Gaussian shape, in good agreement with the experimental as well as simulated data. The velocity necessary to outrun diffusion is given by $v \gtrsim 4D/(L + g)$ for $G_C(\tau) \gtrsim 0.5$, consistent with our earlier analysis.

The effect of flow on correlation is further illustrated by looking at the simpler case of only one detection volume, i.e., by autocorrelation analysis. In Fig. 4, the autocorrelation functions of the same traces used for cross-correlation analysis [Fig. 3(a)] are shown as well as analytically

derived functions [11]. Similar to fluorescence correlation spectroscopy, the functions exhibit a simple shape consisting of a plateau for short times (not fully captured at the limited measurement bandwidth) and an exponential $\tau^{-1/2}$ tail of the correlation which shifts to shorter times with increasing flow. Extrapolating the functions linearly to $G_A = 0$ leads to a time indicating the loss of correlation which is consistent with τ_{peak} (for our case $L \approx g + L$), as shown in Fig. 4(a).
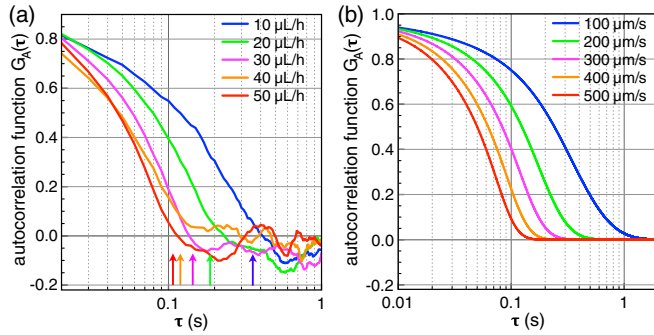
FIG. 4 (color online). (a) Autocorrelation functions deter-
mined of the same traces (but only from one electrode) used
for the cross-correlation analysis. The arrows indicate the cor-
responding cross-correlation peak times shown in Fig. 3(a).
(Functions for smaller flow rates are omitted because the short
duration of the traces leads to excessive scatter.) (b) Analytically
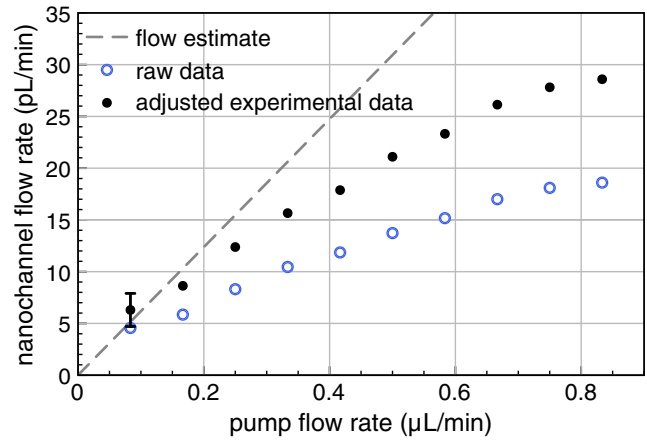derived one-dimensional autocorrelation functions.

FIG. 5 (color online).   Nanofluidic flow rates in a nanofluidic
device as a function of syringe pump flow rate. The adjusted
experimental data points (black dots) include a correction for
adsorption as well as for the shift of the peak times τ_{peak}. The
dashed line's slope is identical to the ratio of hydraulic resis-
tances $2R_{\text{micro}}/R_{\text{nano}} = 1/16\,000$.

As a simple illustrative application, we extract the liquid
flow rate from the cross correlation. In a first approxima-
tion this can be done using the time-of-flight expression
$Q_{\text{nano}} = (L + g)h_n w_n/\tau_{\text{peak}}$. Nanochannel flow rates ob-
tained in this manner are shown in Fig. 5 as a function of
the syringe pump flow rate (blue circles). The molecules'
fast shuttling eliminates the need for velocity corrections
as used in micro particle image velocimetry [14]. Two
effects need to be corrected for an accurate flow rate
determination, however. First, the peak time τ_{peak} deviates
up to 10% from the time-of-flight approximation for slow
flow rates because the peak shape is then strongly influ-
enced by diffusion. This effect is easily corrected by using
the full analytical cross-correlation function, Eq. (4), as
discussed in the Supplemental Material [11]. A second,
more important source of a systematic error is reversible
adsorption of redox-active molecules at the channel walls
and electrodes inherent to the high surface-to-volume ratio
in nanogap devices [6,15]. The fraction of adsorption
$N_{\text{ads}}/N_{\text{tot}}$ and thereby the retardation of the analyte mole-
cules can be readily extracted from the mesoscopic
fluctuation using the expression $N_{\text{ads}}/N_{\text{tot}} = 1 -
h^2\langle\delta I^2\rangle/eD\langle I\rangle$ [15]. By averaging over thirty time traces
we determine a reduction of the molecule's speed to be
$N_{\text{ads}}/N_{\text{tot}} = 35\% \pm 5\%$.

Flow rate data adjusted for both adsorption and the
diffusion-induced peak shift are shown as black dots in
Fig. 5. We attribute the sublinear increase of the nano-
channel flow at high pump flow rates to bulging of the
microchannel (at a pressure drop of approximately 0.5 bar),
an effect that is well known for soft PDMS microchannels
[16,17].

At the lowest pump rates, we measure nanochannel flow
below 10 pL/min, which is below the lowest previously
reported value of ~ 30 pL/min [7].

While the measurements shown here were performed at
a relatively high concentration of 1 mM, the method is in
principle applicable at arbitrarily low concentrations be-
cause other intrinsic sources of noise exhibit the same
scaling with concentration (or, equivalently, average cur-
rent) but with a smaller amplitude [18]. In particular,
at a bandwidth of 10 Hz the rms shot noise and Johnson
noise are $\sqrt{2e \times 10\text{ Hz}}\sqrt{I} = 1.8 \times 10^{-9}\text{ A}^{1/2}\sqrt{I}$ and
$\sqrt{4kT \times 10\text{ Hz}/0.4\text{V}}\sqrt{I} = 6.4 \times 10^{-10}\text{ A}^{1/2}\sqrt{I}$, respec-
tively, whereas the diffusion noise dominates with
$\sqrt{eD/h^2}\sqrt{I} \approx 10^{-7}\text{ A}^{1/2}\sqrt{I}$.

At sufficiently low concentrations, the sensitivity
becomes limited by extrinsic instrumental noise instead.
A single molecule yields a current of $i = eD\epsilon/h^2$ with $\epsilon =
1 - N_{\text{ads}}/N_{\text{tot}}$, and single molecule detection was previ-
ously demonstrated in 70 nm high diffusively coupled
nanogap sensors at $i = 20$ fA with a signal-to-noise ratio
of 1 and an instrumental response time of 100 ms [12]. If
the signal-to-noise ratio could be increased, e.g., by im-
proved instrumentation or reduced channel height, it would
then become possible to distinguish single molecules ac-
cording to their diffusion coefficient, size or charge trans-
fer, or by their electrochemical properties when biasing
successive transducers at different redox potentials.

In conclusion, we have developed electrochemical
cross-correlation spectroscopy as a new technique to study
the transport of mesoscopic numbers of electroactive ana-
lyte molecules in nanofluidic volumes. Here we employed
this method for the determination of record-low liquid flow
rates. We also envision a broader range of applications:
similar to its direct optical analogue, fluorescence (cross-)
correlation spectroscopy [13,19,20], the technique can be
used to investigate local concentration, adsorptivity and

chemical reaction kinetics of analyte molecules. As compared to fluorescence correlation spectroscopy, our method permits studying the properties of a different class of molecules or molecular labels (electrochemically active instead of fluorescent). Furthermore, all-electrical detection without the need for a microscope facilitates integration in microfluidic lab-on-a-chip systems, where multiple detectors in more complex nanochannel networks can also be realized.

---

*s.g.lemay@utwente.nl

[1] D. Magde, E. Elson, and W. W. Webb, Phys. Rev. Lett. **29,** 705 (1972).

[2] E. L. Elson and D. Magde, Biopolymers **13,** 1 (1974).

[3] E. L. Elson and D. Magde, Biophys. J. **101,** 2855 (2011).

[4] M. A. G. Zevenbergen, B. L. Wolfrum, E. D. Goluch, P. S. Singh, and S. G. Lemay, J. Am. Chem. Soc. **131,** 11471 (2009).

[5] Note that there is a strong separation of time scales: due to the high aspect ratio (700:1) geometry of the channel, a molecule crosses the channel vertically within microseconds, but it takes seconds before the longitudinal fluctuation correlation is lost completely.

[6] S. Kang, K. Mathwig, and S. G. Lemay, Lab Chip **12,** 1262 (2012).

[7] H. Liang, W. J. Nam, and S. J. Fonash, in *Technical Proceedings of the NSTI Nanotechnology Conference, Boston, 2008* (CRC, Boca Raton, 2008), Vol. 3, p. 281.

[8] H. Liang, Ph.D. thesis, The Pennsylvania State University, 2008.

[9] H. Bruus, Lab Chip **11,** 3742 (2011).

[10] L. Rassaei, K. Mathwig, E. D. Goluch, and S. G. Lemay, J. Phys. Chem. C **116,** 10913 (2012).

[11] See Supplemental Material at http://link.aps.org/supplemental/10.1103/PhysRevLett.109.118302 for derivation and discussion of an analytical expression for a one-dimensional electrochemical auto- as well as cross-correlation function with flow; overlay of experimentally obtained, simulated, and analytical cross-correlation functions; estimation of electroosmotic backflow in nanochannels; and details on the overall microfluidic circuitry.

[12] M. A. G. Zevenbergen, P. S. Singh, E. D. Goluch, B. L. Wolfrum, and S. G. Lemay, Nano Lett. **11,** 2881 (2011).

[13] M. Brinkmeier, K. Dörre, J. Stephan, and M. Eigen, Anal. Chem. **71,** 609 (1999).

[14] A. Kloostermann, C. Poelma, and J. Westerweel, Exp. Fluids **50,** 1587 (2010).

[15] P. S. Singh, H.-S. M. Chan, S. Kang, and S. G. Lemay, J. Am. Chem. Soc. **133,** 18289 (2011).

[16] M. A. Holden, S. Kumar, A. Beskok, and P. S. Cremer, J. Micromech. Microeng. **13,** 412 (2003).

[17] T. Gervais, J. El-Ali, A. Günther, and K. F. Jensen, Lab Chip **6,** 500 (2006).

[18] P. Horowitz and W. Hill, *The Art of Electronics* (Cambridge University Press, Cambridge, England, 1989).

[19] D. Magde, W. W. Webb, and E. L. Elson, Biopolymers **17,** 361 (1978).

[20] P. S. Dittrich and P. Schwille, Anal. Chem. **74,** 4472 (2002).

Supplemental Material for:
Electrical Cross-Correlation Spectroscopy:
Measuring Picoliter-per-Minute Flows in Nanochannels

Klaus Mathwig, Dileep Mampallil, Shuo Kang, and Serge G. Lemay

MESA+ Institute for Nanotechnology, University of Twente, PO Box 217,
7500 AE Enschede, The Netherlands

A Analytical determination of an autocorrelation function

We derive an analytical expression for a cross-correlation function (CCF) for molecular number fluctuations in electrochemical correlation spectroscopy (ECS) [1] in close analogy to fluorescence (auto-)correlation spectroscopy (FCS) as found in textbooks [2,3]. For both ECS and FCS a correlation function is defined as

$$G(\tau) = \frac{\langle \delta I(t) \delta I(t+\tau) \rangle}{\langle I(t) \rangle^2}. \tag{1}$$

$I(t)$ is the measured current or fluorescence intensity, respectively, with the fluctuation $\delta I(t) = I(t) - \langle I(t) \rangle$ and $\langle I(t) \rangle = 1/T \int_0^T I(t) \mathrm{d}t$. In both cases $I(t)$ and $\delta I(t)$ are defined as

$$I(t) = Q \int W(\mathbf{r}) n(\mathbf{r}, t) \mathrm{d}\Omega \quad \text{and} \quad \delta I(t) = Q \int W(\mathbf{r}) \delta n(\mathbf{r}, t) \mathrm{d}\Omega \tag{2}$$

with $W(\mathbf{r})$ being the sample region, $n(\mathbf{r}, t)$ the analyte number per volume and $\mathrm{d}\Omega$ a volume element. In FCS, Q is a function of fluorescence quantum efficiency, collection efficiency and adsorptivity. In the case of redox cycling, we define Q as the faradaic current per electrochemically active molecule, i.e. as a function of the elementary charge e and the time h^2/D it takes for one molecule to travel back and forth between the two electrodes by diffusion:[1]

$$Q = eD/h^2. \tag{3}$$

Here D is the analyte's diffusion coefficient and h the channel height. Typically Q is in the order of 10^{-14} A for the nanofluidic devices employed here.

In FCS, the sample region $W(\mathbf{r})$ is the product of the spatial intensity profile of the excitation light source, the sample extent and the volume from which fluorescence is measured. Typically, W has the form of a three-dimensional Gaussian profile determined by the laser focus of a confocal microscope. In ECS, each detection region is simply

---

[1]This equation is only correct for a high overpotential leading to a diffusion-limited faradaic current, a concentrated background electrolyte that prevents any electrical migration, and a redox reaction in which only one electron is transferred.
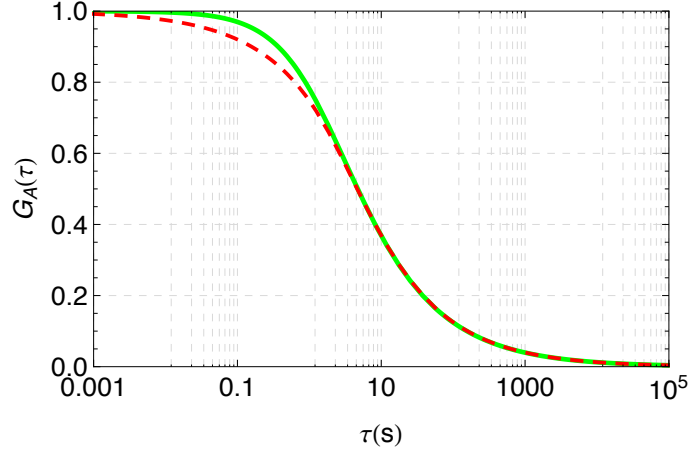
Figure S1: Analytically derived autocorrelation function $G_A(\tau)$ (eq. (7), dashed red curve) for $D = 5 \cdot 10^{-10}\,\mathrm{m^2/s}$ and $L = 100\,\mu\mathrm{m}$. It is compared to one-dimensional diffusion across a Gaussian focus, i.e. $G_A(\tau) = 1/\sqrt{(1 + 4D\tau/L^2)}$ (green curve) with $D = 5 \cdot 10^{-10}\,\mathrm{m^2/s}$ and $L = 56\,\mu\mathrm{m}$.

a box, i.e. the nanochannel volume confined in between the top and bottom electrode (channel/electrode size L, w, h):

$$W(\mathbf{r}) = \begin{cases} 1, & 0 \leq x \leq L, 0 \leq y \leq w, 0 \leq z \leq h, \\ 0, & \text{otherwise.} \end{cases} \tag{4}$$

In the case of both FCS and ECS, the autocorrelation function is evaluated by

$$G_A(\tau) = \frac{\int \int W(\mathbf{r})W(\mathbf{r}')f(\mathbf{r}, \mathbf{r}', \tau)\mathrm{d}\Omega\mathrm{d}\Omega'}{(\langle n \rangle \int W(\mathbf{r})\mathrm{d}\Omega)^2}. \tag{5}$$

f denominates the correlation of the number concentration fluctuation at position $\mathbf{r}$ with a number fluctuation at position $\mathbf{r}'$ at a time τ earlier, i.e. $f(\mathbf{r}, \mathbf{r}', \tau) = \langle \delta n(\mathbf{r}, \tau)\delta n(\mathbf{r}', 0) \rangle$. It is evaluated by solving the diffusion equation $\partial f/\partial\tau = D\nabla^2 f$ and has the form

$$f = \frac{1}{(4\pi D\tau)^{d/2}}\exp\left(-\frac{|\mathbf{r} - \mathbf{r}'|^2}{4D\tau}\right)\langle n \rangle \tag{6}$$

in $d = 1, 2, 3$ dimensions.

We analytically solve equation (5) in one dimension along the nanochannel. Our system allows for this simplification because the molecules' lateral and vertical diffusion is confined by channel walls and electrodes and takes place on timescales which are too short to be experimentally accessible.

The simple form of the sample region W (eq. (4)) simplifies the integrals, e. g. $\int_{-\infty}^{\infty} W\mathrm{d}x = 1/L \int_0^L 1\mathrm{d}x = 1$. The normalized ACF (i.e. normalized to 1 at $\tau{=}0$ by multiplying by the
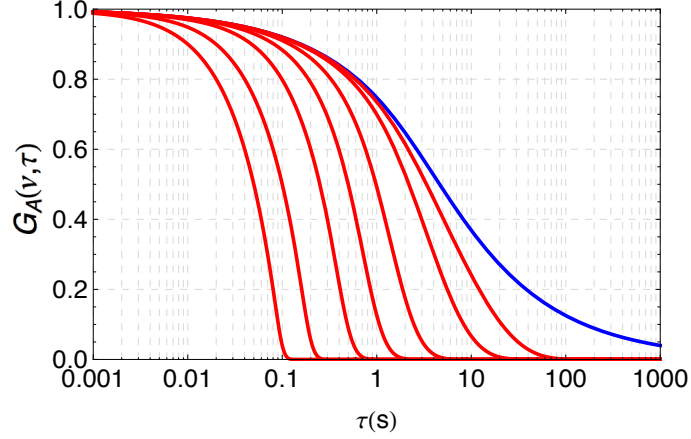
Figure S2: Autocorrelation function $G_A(\tau)$ (eq. (9)) for $D = 5 \cdot 10^{-10}\,\mathrm{m^2/s}$ and $L = 100\,\mu\mathrm{m}$ and flow velocities ranging from $v = 1\,\mathrm{mm/s}$ to $10\,\mu\mathrm{m/s}$ (red curves, from left to right) and no flow (blue curve).

absolute number of active molecules $\langle n \rangle L$) is then of the form

$$G_A(\tau) = \sqrt{\frac{4D\tau}{L^2\pi}} \left(\exp\left(-\frac{L^2}{4D\tau}\right) - 1 \right) + \mathrm{erf}\left(\frac{L}{\sqrt{4D\tau}}\right). \tag{7}$$

In Figure S1 the function $G_A(\tau)$ is shown and compared to a typical Fluorescence ACF of one-dimensional diffusion through a 3-D Gaussian focus.

B Autocorrelation including flow

When flow with a mean velocity v is introduced in a nanochannel (or an FCS focus), the number correlation function f can no longer be evaluated by solving a diffusion equation, but a Fokker-Planck equation $\partial f / \partial \tau = D\nabla^2 f - \mathbf{v} \cdot \nabla f$ with $\mathbf{v}$ being the flow velocity has to be used instead [4]. For the one-dimensional case, f is

$$f = \frac{1}{(4\pi D\tau)^{1/2}} \exp\left(-\frac{|x - x' - v\tau|^2}{4D\tau}\right) \langle n \rangle. \tag{8}$$

The normalized autocorrelation function $G_A(\tau, v)$ is then derived as shown above. The end result has the form

$$G_A(\tau) = \sqrt{\frac{D\tau}{L^2\pi}} \left(\exp\left(-\frac{(L + v\tau)^2}{4D\tau}\right) + \exp\left(-\frac{(L - v\tau)^2}{4D\tau}\right) - 2\exp\left(-\frac{(v\tau)^2}{4D\tau}\right) \right) +$$

$$\frac{L + v\tau}{2L} \mathrm{erf}\left(\frac{L + v\tau}{\sqrt{4D\tau}}\right) + \frac{L - v\tau}{2L} \mathrm{erf}\left(\frac{L - v\tau}{\sqrt{4D\tau}}\right) - \frac{v\tau}{L} \mathrm{erf}\left(\frac{v\tau}{\sqrt{4D\tau}}\right). \tag{9}$$

It is shown in Figure S2 (similar to Figure 4b in the main article) for different flow velocities. With increasing flow speed, the residence time of molecules in the nanochannel is reduced and the correlation is lost at increasingly shorter times τ.
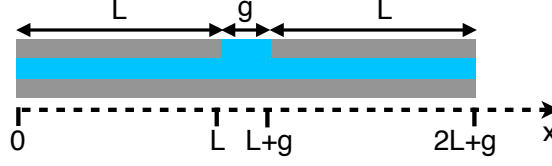
Figure S3: Geometry and integration boundaries for determining a cross-correlation function. Two top electrodes of the length L are separated by a gap g. Liquid is flowing from left to right.

C Analytical cross-correlation function

We derive the analytical form of an electrochemical cross-correlation function $G_C(\tau)$ with and without flow in the same way as the autocorrelation function shown above – the only difference being that two geometrically separated detection volumes W_1 and W_2 (corresponding to the two top electrodes) are being correlated with each other instead of just one volume being correlated with itself. The cross-correlation function $G_C(\tau) = \langle \delta I_1(t) \delta I_2(t + \tau) \rangle / (\langle I_1(t) \rangle \langle I_2(t) \rangle)$ is then evaluated by

$$G_C(\tau) = \frac{\int \int W_1(\mathbf{r}) W_2(\mathbf{r}') f(\mathbf{r}, \mathbf{r}', \tau) \mathrm{d}\Omega \mathrm{d}\Omega'}{\langle n \rangle^2 \int W_1(\mathbf{r}) \mathrm{d}\Omega \int W_2(\mathbf{r}') \mathrm{d}\Omega'}. \tag{10}$$

The electrode geometry and integration boundaries are shown in Figure S3. For two identical top electrodes with a length L and a gap of length g in between them, the numerator of eq. (10) reads

$$\int \int W_1(\mathbf{r}) W_2(\mathbf{r}') f(\mathbf{r}, \mathbf{r}', \tau) \mathrm{d}\Omega \mathrm{d}\Omega' = \int_0^L \int_{L+g}^{2L+g} f(x, x', \tau) \mathrm{d}x \mathrm{d}x'. \tag{11}$$

Using the number concentration fluctuation function including a flow velocity v (eq. (8)), the normalized cross correlation function $G_C(\tau, v)$ can be explicitly expressed as:

$$G_C(\tau) = \sqrt{\frac{D\tau}{\pi L^2}} \left(\exp\left(-\frac{(2L + g - v\tau)^2}{4D\tau} \right) + \exp\left(-\frac{(g - v\tau)^2}{4D\tau} \right) - 2\exp\left(-\frac{(L + g - v\tau)^2}{4D\tau} \right) \right)$$

$$+ \frac{2L + g - v\tau}{2L} \operatorname{erf}\left(\frac{2L + g - v\tau}{\sqrt{4D\tau}} \right) + \frac{g - v\tau}{2L} \operatorname{erf}\left(\frac{g - v\tau}{\sqrt{4D\tau}} \right)$$

$$- \frac{L + g - v\tau}{L} \operatorname{erf}\left(\frac{L - g + v\tau}{\sqrt{4D\tau}} \right). \tag{12}$$

$G_C(\tau)$ is shown in Figure S4 for different flow velocities v. The times τ_{peak} of the peak maxima correspond to the times of flight of the analyte molecules from the center of one electrode to the other electrode downstream. τ_{peak} shifts to shorter times with increasing flow velocity. For slower velocities, the correlation is increasingly lost during the flight due to longitudinal diffusion. This leads to shallower peaks.
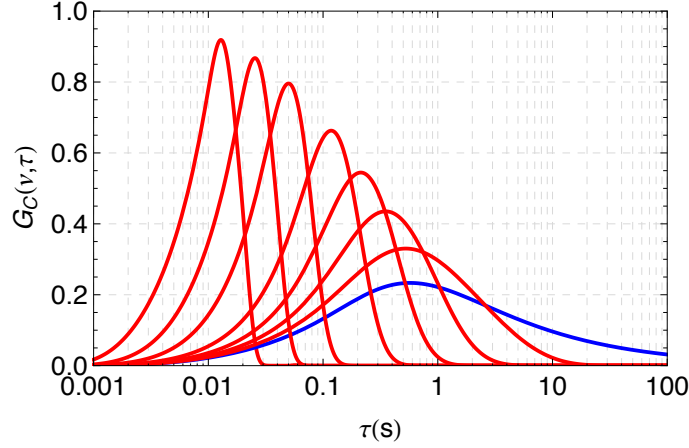
Figure S4: Cross-correlation function $G_C(\tau)$ (eq. (12)) for $D = 5 \cdot 10^{-10}\,\mathrm{m}^2/\mathrm{s}$, $L = 24\,\mu\mathrm{m}$ and $g = 2\,\mu\mathrm{m}$ and flow velocities ranging from $v = 2\,\mathrm{mm/s}$ to $20\,\mu\mathrm{m/s}$ (red curves, from left to right) and no flow (blue curve).

Note that in contrast to Figure 3 in the main article, a shorter electrode length of $L = 24\,\mu\mathrm{m}$ instead of $49\,\mu\mathrm{m}$ is used in Figure S4. Therefore the correlation is lost more quickly with decreasing flow rate. This effect was also confirmed by experiment as well as random walk simulations (data not shown).

For low flow velocities, the increasing influence of diffusion on the cross-correlation function's peak shape shifts the peak times τ_{peak} away from the actual times of flight towards shorter times τ. This effect also exists in fluorescence cross correlation spectroscopy [5]. We quantify it by dividing the times τ_{peak} of the cross-correlation peaks shown in Figure S4 by the corresponding times of flight $(L + g)/v$. This fraction as a function of the flow velocity is shown in Figure S5. For any data shown in the main article, τ_{peak} does not deviate more than 10% from the time of flight.

D Overlay of cross-correlation functions

An overlay of the experimentally obtained, simulated and analytical cross-correlation functions already shown in Figure 3 in the main article is shown in Figure S6 for the illustrative flow rate of $50\,\mu\mathrm{L/h}$ and flow velocities of $500\,\mu\mathrm{m/s}$ respectively. The curves show good agreement.

E Determining the influence of the streaming potential

Pressure-driven flow can cause advection of mobile counterions in the diffuse part of the electric double layer, consequently inducing a streaming potential gradient between
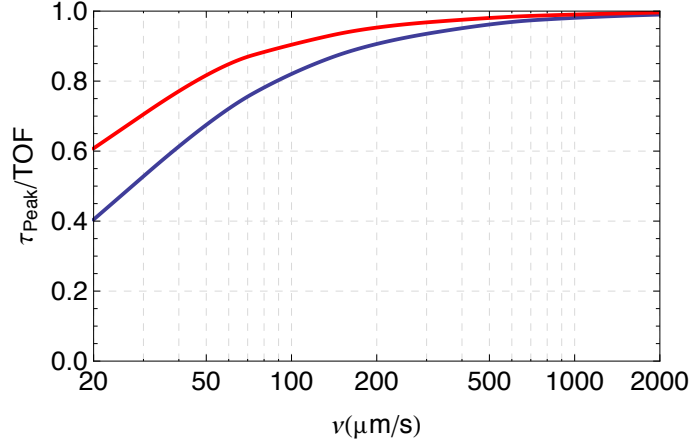
Figure S5: Deviation of the cross-correlation function's peak time τ_{peak} from the time of flight as a function of flow velocity for the experimental parameters $D = 5 \cdot 10^{-10}\,\text{m}^2/\text{s}$, and $g = 2\,\mu\text{m}$ and two different electrode lengths of $L = 24\,\mu\text{m}$ (blue curve) and $L = 49\,\mu\text{m}$ (red curve).

the two ends of the channel. The corresponding streaming potential field induces an electroosmotic back transport that opposes the pressure-driven flow [6]. We calculate the magnitude of the streaming potential difference for a one-dimensional channel with height h and length L containing a electrolyte of conductivity K as

$$V_s = \frac{\varepsilon \zeta}{\eta K} \Delta p, \tag{13}$$

where ε is the permittivity of the liquid, ζ is the zeta potential of the walls, Δp is the pressure gradient applied across the nanochannel and η is the viscosity. We consider the following parameters: $L = 100\,\mu\text{m}$, $z = 130\,\text{nm}$, aqueous solution as the electrolyte with conductivity $10\,\text{S/m}$ (for a $1\,\text{M}$ concentration of KCl), ζ in the order of magnitude of $-10\,\text{mV}$, $\eta = 0.001\,\text{Pa s}$ and a pressure difference $\Delta p = 1\,\text{bar}$. This gives a streaming potential of $V_s = 7\,\mu\text{V}$. We assume that V_s drops along the channel length L resulting in an electroosmotic back flow

$$u_{eo} = \frac{\varepsilon \zeta}{\eta} \frac{V_s}{L}. \tag{14}$$

The magnitude of u_{eo} is determined as $0.5\,\text{nm/s}$, which is negligible compared to the applied pressure driven flow velocity of several $\mu\text{m/s}$.
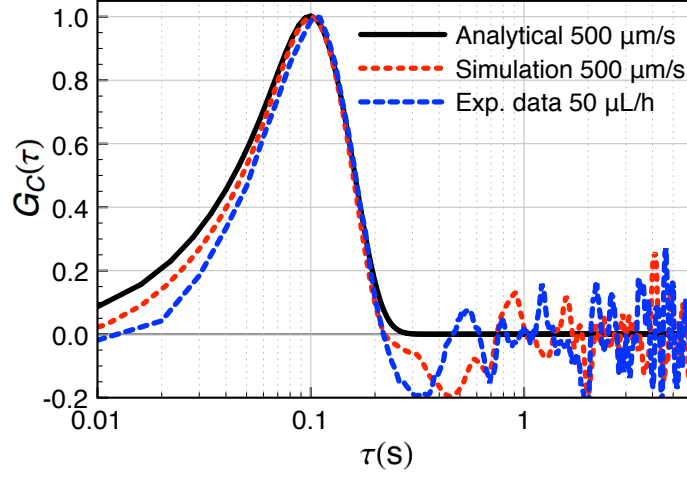
Figure S6: Overlay of an experimentally determined cross-correlation function for an overall flow rate of $50\,\mu\mathrm{L/h}$, and the simulated function and analytical solution for an average flow velocity of $500\,\mu\mathrm{m/s}$. All curves are normalized to a peak height of 1.

F Microfluidic channels

A micrograph of the overall fluidic circuitry is shown in Figure S7. Two nanofluidic devices were connected simultaneously by microchannels in a polydimethylsiloxane (PDMS) layer bonded (after activation in an oxygen plasma) to the chip. Small holes were cored in the PDMS before bonding. Tubing can be reversibly connected to these holes to connect the chip to the syringe pump as well as the reference electrode. The tubing connected to the reference electrode downstream can be reversely purged with $1\,\mathrm{M}$ KCl solution to avoid slow filling of its large dead volume through the PDMS microchannel. The wide fluidic channels in PDMS leading to the smaller parallel nano- and microchannels are designed $500\,\mu\mathrm{m}$ wide in order to maximize the pressure drop at the devices, and thereby minimize the absolute pressure drop at high flow rates and to prevent leakage or breaking of the PDMS-silicon nitride bond. Being only $3\,\mu\mathrm{m}$ high, the channels have a cross-section with a very low aspect ratio and an array of PDMS pillars within the channels is used to stabilize them mechanically and prevent collapse. We estimate that about 70% of the overall pressure drops across the narrow micro- and nanochannels. The fluidic resistance of the tubing is negligible.
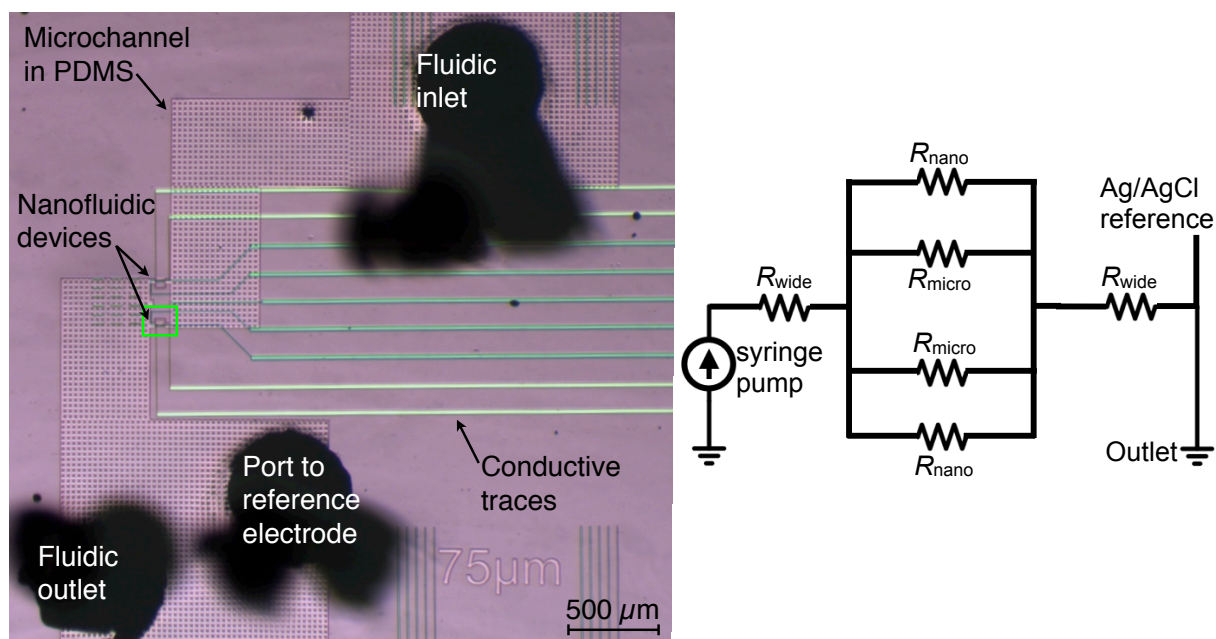
Figure S7: Microfluidic circuitry. Left: Micrograph of a fluidic chip with PDMS bonded on top. The green square marks the image detail shown in Figure 2c in the main article. Right: Equivalent circuit diagram of the fluidic channels.

References

[1] M. A. G. Zevenbergen, B. L. Wolfrum, E. D. Goluch, P. S. Singh, and S. G. Lemay, J. Am. Chem. Soc. **131**, 11471 (2009).

[2] J. Enderlein, *Handbook of Single-Molecule Biophysics*, edited by P. Hinterdorfer and A. V. Oijen (Springer, New York, 2009).

[3] N. L. Thompson, *Topics in Fluorescence Spectroscopy, Volume 1: Techniques*, edited by J. R. Lakowicz (Plenum Press, New York, 1991).

[4] D. Magde, W. W. Webb, and E. L. Elson, Biopolymers **17**, 361 (1978).

[5] P. S. Dittrich and P. Schwille, Anal. Chem. **74**, 4472 (2002).

[6] D. Burgreen and F. R. Nakache, J. Phys. Chem. **68**, 1084 (1964).